# Medical Image Registration and Fusion Using Principal Component Analysis

Meisen Pan, Jianjun Jiang, Fen Zhang, and Qiusheng Rong
College of Computer Science and Technology, Hunan University of Arts and Science, China

**Abstract**: *Principal Component Analysis* (*PCA*) *is widely used in the field of medical image processing. In this paper, PCA is applied to align and fuse the images. When alignment, first, the centroids of the static and moving images are derived by computing the image moments and taken as the translation values for registration, then the subtraction of two rotation angles produced by using PCA to solve the covariance matrice of image coordinates is counted as the rotation values for registration, finally the moving image is aligned with the static one. The Closest Iterative Point* (*ICP*) *algorithm exists some problems which worth improving. Therefore, we combine PCA with ICP to align the images in this paper. The translation and rotation values derived by PCA are views as the initial request parameters of ICP, which is conducive to further advancing the registration accuracy. The experimental results show that the combination method has a fairly simple implementation, low computational load, good registration accuracy, and also can efficiently avoid trapping in the local optima. When fusion, a slipping window with size being* $Size \times Size$ *is first moved across the fusing images to construct sub-block with size also being* $Size \times Size$*, then the eigenvectors of the covariance matrix created by using PCA to each sub-block are acquired, finally the absolute values of the eigenvectors are added to compute the fusion coefficient of the central pixel of each sub-block and the images are fused. The results reveal that this proposed fusion method is superior to the traditional PCA-based image fusion.*

**Keywords**: *Centroids, image registration, principal component analysis, image fusion*.

*Received October 14, 2014; accepted May 19, 2015*

## 1. Introduction

Medical image registration, as the prerequisite for medical image fusion, signifies that by means of computer technology, a kind of or A series of spatial geometric transform is/are performed on two or more images created by various imaging devices such Magnetic Resonance Imaging (MRI), Positron Emission Tomography (PET), Single-Photon Emission Computed Tomography (SPECT) and so forth, and this makes the pixels (voxels) expressing the identical structure to achieve the space correspondence [15, 16]. In recent years, following the development of medical imaging technology, the medical image registration has been turned into a research focus which has been alluring increasing attention. In the last decades, the methods for registering medical images have achieved rapid advance, and global experts and scholars have proposed many practical and effective technologies. Among these methods, feature-based image approaches have been extensively applied for aligning medical images [11, 12]. For the feature-based image registration, in essence, it extracts the common, distinct and significant features between the aligning images to explore the transformation parameters. It is effective and easy to implement, but its registration accuracy seriously counts on whether it can exactly extract the critical feature points [3, 10, 17]. In consideration of the complexity of various medical images, it is an intractable issue to solve the automatically and accurately abstract and refine the useful feature points from medical images. So its poor adaptability and robustness need to be further boosted. The Closest Iterative Point (ICP) algorithm, as a feature-based registration method, is a very famous method and widely put into use in the registration of point sets [1, 2, 7]. However, it exists some problems that need to be resolved in the implement process. First, it must repetitively and iteratively explore the closest points, and as a result the computation costs are extremely expensive. Second, whether ICP can exactly derive the optimal registration parameters seriously dependent on the selection of the initial rotation and translation values. If the initial values are ill-fitted to respond to ICP, then the registering operation needs more exploring time and even fails. Third, it is troublesome to automatically select the pivotal feature points delineating the image outline in image alignment. Furthermore, it easily falls into the trap of the local optima.

The objective of image fusion is to combine various information from source images produced by using different sensors to sample the same scene, and achieve a new image which can provides much more visual information than the source images. Image fusion, as a effective information fusion technology, has been extensively applied in many fields such as remote sensing image processing, object recognition, medical science, computer vision and so on [9, 13]. In recent years, the experts around the world have

proposed many fusion methods. In sum, these methods are divided into three levels: pixel-, feature- and decision-based fusions. Among them, pixel-based fusion is the most essential one and is also the foundation of other two levels. Thus research about pixel-based fusion is the crucial point and includes many algorithms such as the weighted average fusion, the pyramid decomposition fusion, the wavelet transform fusion and so on. Although these algorithms can achieve good fusion effect, they have less consideration of image edge information and regional feature [4, 18].

There is a close relationship between image registration and fusion, especially for multi-modality medical image, registration and fusion are inextricably linked. In the course of image fusion processing, image registration is the first step and the precondition. Only when the alignment of the fusing images comes true will the corresponding tissues in the images be accurately merged. On the contrary, if there are obvious location deviations between the corresponding tissues, then the image fusion is unreliable and inaccurate result. Therefore, medically speaking, the fused image covers meaningful and useful information when the same space location in the fusing images is in accordance with the corresponding anatomy structure.

On the foundation of an in-depth research about the Principal Component Analysis (PCA), we use PCA to align and fuse the medical image. When aligning the images, first, by using the image moments the centroids of the static and moving images are counted to obtain the translation values. Second, the medical image coordinates are centralized to move the coordinate origin to the centroid location, the two-row coordinate matrix is produced and used to acquire the covariance matrix, the eigenvectors are derived to form the transformation kernel matrix, the arcsine is solved to obtain the rotation angle, and rotation angles of two images are subtracted to get the rotation value. Finally, the translation and rotation values acquired by the method above are used to register the images. When fusing the images, we propose medical image Fusion using Modified Principal Component Analysis (FMPCA) to deal with image fusion. First, a Size×Size window is moved across the fusing images to construct sub-block with size also being Size×Size, and the covariance matrix of each sub-block is solved respectively by PCA to obtain the eigenvectors. Second, the absolute values of the eigenvectors are added to compute the fusion coefficient of the central pixel of each sub-block. Finally the image fusion operation is performed.

## 2. Medical Image Registration Using PCA

### 2.1. Acquisition of the Centroids of the Medical Image

For a 2-D discrete function $f(x, y)$, the moment of order $(p+q)$ can be defined by [6, 19].

$$M_{p,q} = \sum_{x=1}^{M} \sum_{y=1}^{N} x^p y^q f(x,y) \qquad p,q = 0,1,2,... \tag{1}$$

Where $(p+q)$ is the order of the moment and, $M$ and $N$ represent the numbers of sampling points in space. And well we can define the zeroth moment as follows [6, 19].

$$M_{0,0} = \sum_{x=1}^{M} \sum_{y=1}^{N} f(x,y) \tag{2}$$

Further, when $p$=1 and $q$=0, and, $p$=0 and $q$=1 [6, 19],

$$\bar{x} = \frac{M_{1,0}}{M_{0,0}}, \quad \bar{y} = \frac{M_{0,1}}{M_{0,0}} \tag{3}$$

here $(\bar{x}, \bar{y})$ is defined as the centroid coordinates of the object.

When aligning images, we compute the zeroth and first-order moments of static image $S$ and moving image $M$ respectively by using Equations 1, 2, and 3, and then procure the centroids $(\bar{x}_s, \bar{y}_s)$ and $(\bar{x}_m, \bar{y}_m)$.

### 2.2. Calculation of the Rotation Angle of the Medical Image using PCA

PCA, also called Karhunen-Loeve Transform (KLT), is an orthogonal transform based on the statistical feature and has been used extensively in the field of image processing. In this paper, suppose that $Y \in R^{2\times J}$ and $yi=[y_{i1}\ y_{i2}]^T$ $(i=1, 2, ..., J)$ is an element of the vector set $Y$, and then the eigenvectors of the covariance matrix of $Y$ is invariant to rotation transformation.

*Proof.* Let matrix $Y$ be rotated by the angle Θ, the rotation matrix is expressed:

$$R = \begin{bmatrix} \cos\theta & \sin\theta \\ -\sin\theta & \cos\theta \end{bmatrix}, \tag{4}$$

Then

$$RR^T = \begin{bmatrix} \cos\theta & \sin\theta \\ -\sin\theta & \cos\theta \end{bmatrix} \begin{bmatrix} \cos\theta & \sin\theta \\ -\sin\theta & \cos\theta \end{bmatrix}^T = \begin{bmatrix} 1 & 0 \\ 0 & 1 \end{bmatrix}, \tag{5}$$

and $Y_R=YR$ . $M_{Y_R}$ is the mean vector of $Y_R$ and is expressed as follows:

$$M_{Y_R} = E\{Y_R\} \tag{6}$$

where $E\{.\}$ is the expected value of the argument. $Cov_{Y_R}$ is the covariance matrix of set $Y_R$ and is given by the expression

$$\begin{aligned} \mathrm{Cov}_{Y_R} &= \mathrm{E}\{Y_R Y_R^T\} = \mathrm{E}\{(YR)(YR)^T\} \\ &= \mathrm{E}\{YRR^T Y^T\} = \mathrm{E}\{Y(RR^T)Y^T\} \\ &= \mathrm{E}\{Y^T Y\} = \mathrm{Cov}_Y \end{aligned} \tag{7}$$

From Equation (5) we know, the covariance matrix of $Y_R$ is the same as that of $Y$, which means that they have the same eigenvalues and eigenvectors. Therefore, the eigenvectors of the covariance matrix of $Y$ are invariant to rotation transformation, which is to be proved.

According to the process of PCA, the eigenvectors of the covariance matrix are obtained and then are formed into the kernel matrix $A=\begin{bmatrix} e_{11} & e_{12} \\ e_{21} & e_{22} \end{bmatrix}$, in which the value $e_{11}$ is used to compute the arcsine value and the rotation angle is obtained. As mentioned before, the method for acquiring the rotation angle from the moving image $s$ by PCA is listed as bellow.

- *Step 1*. The image matrix $P_s$ is built, namely, the origin of coordinates is moved to the centroids of the image $s$, which means that the coordinates of the image $s$ are centralized. $P_s$ denotes the two-row matrix of the coordinates ($x$, $y$) in the image $S$, where the number of elements (i.e., the number of columns) is $M \times N$, that is, $Ps \in R^{2\times(M\times N)}$.

$$\begin{cases} p_S(1,(i-1)\times N+j) = (i-\overline{x_S})\times s(i,j) \\ p_S(2,(i-1)\times N+j) = (j-\overline{y_S})\times s(i,j) \end{cases} \quad (8)$$

here $i$=1, 2, ...., $M$; $j$=1, 2, ..., $N$.

- *Step 2*. The matrix $P_s$ is performed by the following operations

$$\begin{cases} \overline{x_P} = \frac{1}{M\times N}\sum_{i=1}^{M\times N} p_S(1,i) \\ \overline{y_P} = \frac{1}{M\times N}\sum_{i=1}^{M\times N} p_S(2,i) \\ \overline{p_S}(1,i) = p_S(1,i) - \overline{x_P} \ (i=1,2,...,M\times N) \\ \overline{p_S}(2,i) = p_S(2,i) - \overline{y_P} \ (i=1,2,...,M\times N) \end{cases} \quad (9)$$

- *Step 3*. By using PCA, the covariance matrix of $\overline{P_S}$ is solved and the transformation kernel matrix $A_s$ is got.
- *Step 4*. According to $A_s$, the rotation angle $\theta_s$ is obtained:

$$\theta_s = arcsin(e_{11}) \times \frac{180}{\pi} \quad (10)$$

In this paper, the rotation angle $\theta_M$ of the static image $M$ is procured by the method above.

### 2.3. Procedure of Medical Image Registration using PCA

According to the description above, medical image Registration Using Principal Component Analysis (RPCA) is explained as follows.

- *Step 1*. By computing the centroids of the static image $s$ and the moving image $M$, the translation parameters for registration are derived, namely

$$\Delta x = \overline{x}_m - \overline{x}_s \ , \quad \Delta y = \overline{y}_m - \overline{y}_s \quad (11)$$

- *Step 2*. By using KLT, the rotation parameters for registration are acquired, namely

$$\Delta\theta = \theta_m - \theta_S \quad (12)$$

- *Step 3*. The moving image $s$ is translated by $(-\Delta x,-\Delta y)$ and rotated by $-\Delta\theta$, which means that the alignment of tow images are performed.

Although RPCA can complete the image alignment, its accuracy needs to further be boosted. Therefore, we incorporate RPCA with ICP to tackle the image alignment. Due to the existing problems mentioned above, we first use PCA to produce the translation and rotation values $\Delta x$, $\Delta y$ and $\Delta\theta$ as the initial parameters $T_0^0$ and $R_0^0$ of ICP, then use BSGO [16] to extract the feature points and obtain the static and moving point sets of ICP, finally carry out the image registration. In conclusion, Medical Image Registration Using PCA and ICP (RPCA-ICP) is introduced as follows.

- *Step 1*. Compute the centroids $(\overline{x}_s, \overline{y}_s)$ and $(\overline{x}_m, \overline{y}_m)$, and, the rotation angles $\alpha_s$ and $\alpha_m$ of static image $s$ and the moving image $M$ respectively according to the image moments and RPCA.
- *Step 2*. Derive the initial values $\Delta x$, $\Delta y$ and $\Delta\theta$ for registration according to Equations (9) and (10).
- *Step 3*. Use $\Delta x$, $\Delta y$ and $\Delta\theta$ as the initial translation and rotation parameters for ICP, namely

$$T_0^0 = [\Delta x \quad \Delta y]^T, \ R_0^0 = \begin{bmatrix} cos(\Delta\theta) & -sin(\Delta\theta) \\ sin(\Delta\theta) & cos(\Delta\theta) \end{bmatrix} \quad (13)$$

- *Step 4*. Impose BSGO on $s$ and $M$ respectively, and then generate the binarized images $B_s$ and $B_M$ with gray value being 0 or 1.
- *Step 5*. Extract two point sets of coordinates representing all the pixels with gray value being 1 in the images $B_s$ and $B_M$ respectively as the static and moving point sets in ICP.
- *Step 6*. Perform ICP and derive the final rotation and translation matrices $R_0^{k+1}$ and $T_0^{k+1}$.

## 3. Medical Image Registration Using PCA

### 3.1. Traditional Medical Image Fusion using PCA

The rationale of the traditional medical image Fusion using Principal Component Analysis (FPCA) [5, 14] is that the covariance matrices of the fusing images are first computed, then the eigenvalues and eigenvectors are solved, finally the fusion coefficient between the fusing images is determined by the eigenvectors and the images are merged. Supposing there are $m$ source images $I_t(t=1,2,\ldots,m)$ with size being $M\times N$ pixels and its top-left corner pixel is (1, 1). More specifically, FPCA is explained as follows.

- *Step 1*. For each fusing image $I_t$, the column vector is built in row- or column-major order. That is,

$$I_t = \begin{bmatrix} i_t(1,1) & \cdots & i_t(1,N) \\ \vdots & \vdots & \vdots \\ i_t(1,N) & \cdots & i_t(M,N) \end{bmatrix} \quad (14)$$

is turned into the column vector $C_t=[i_t(1,1),...,i_t(M,1),i_t(2,1),...,i_t(M,N)]^T$ $(t=1,2,...,m)$ with size being $MN\times1$, and then a $MN\times m$ vector $C$ is constructed with the column vectors of the $m$ fusing images.

$$C = \begin{bmatrix} C_1 & \cdots & C_t \end{bmatrix} \quad (15)$$

- *Step 2*. The covariance matrix *Cov* is derived by imposing PCA on *C*.
- *Step 3*. The eigenvalue matrix *V* and the eigenvector matrix *D* are solved according to *Cov*, with sizes all being $m\times m$.
- *Step 4*. The first principal component $V_k$ is determined according to the eigenvector matrix *D*.

$$V_k = \begin{bmatrix} V(1,k) \\ \vdots \\ V(m,k) \end{bmatrix} \quad (16)$$

- *Step 5*. The fusion coefficient $V_k$ of each fusing image is:

$$W_t = \frac{V(t,k)}{\sum_{i=1}^{m} V(i,k)} (t = 1,2,...,m) \quad (17)$$

- *Step 6*. $m$ images are merged and the final fused image is created

$$I = \sum_{t=1}^{m} I_t \bullet W_t \quad (18)$$

From the process above, we can find that, the fusion coefficients determined by FPCA are similar to the mean coefficients when there are very minor alterations among the fusing images. However, FPCA can distribute the fusion coefficients more reasonably when there are certain differences among the fusing images. In addition, FPCA cannot accurately allocate the fusion coefficients and even create the serious distortion of the fused image when there are huge divergences among the fusing images (Namely, the little correlations among the fusing images).

### 3.2. Medical Image Fusion using Modified PCA

In FMPCA, the window with size being $Size\times Size$ ($Size$ is an odd.) is first moved across each fusing image to form the sub-block $Block_t^{(i,j)}$ centralizing at the location $(i, j)$ with the same size as the window; for each $Block_t^{(i,j)}$, its covariance matrix is solved and its eigenvalues and eigenvectors are computed. Second, the fusion coefficient $Weight_t^{(i,j)}$ of the central pixel of each $Block_t^{(i,j)}$ is derived from the eigenvalues and eigenvectors. Finally, the pixel value $I(i, j)$ in the fused image $I$ is acquired. In particular, FMPCA is listed as follows.

- *Step 1*. Let the moving window size be $Size\times Size$ and $Es=integer[size/2]$ used for expanding the fusing images.
- *Step 2*. For each $I_t$ with size being $M\times N$, it is expanded by the following rule to the fusing $I_t$ with size being $(M+2*Es)\times(N+2*Es)$.

  1. The original fusing image $I_t$ is expanded the fusing image $I_t$

$$I_t'(Es+1:1:M+Es, Es+1:1:N+Es) = I_t \quad (19)$$

  2. The first $Es$ rows of the image $I_t$ is filled

$$\begin{aligned} &I_t'(1:1:Es, 1:1:N+2*Es) \\ &= I_t'(Size:-1:Es+2, 1:1:N+2*Es) \end{aligned} \quad (20)$$

  3. The last $Es$ rows of the image $I_t$ is filled

$$\begin{aligned} &I_t'(M+2*Es:-1:M+Es+1, 1:1:N+2*Es) \\ &= I_t'(M+2*Es-Size+1:1:M+Es-1, 1:1:N+2*Es) \end{aligned} \quad (21)$$

  4. The first $Es$ columns of the image $I_t$ is filled

$$\begin{aligned} &I_t'(1:1:M+2*Es, 1:1:Es) \\ &= I_t'(1:1:M+2*Es, Size:-1:Es+2) \end{aligned} \quad (22)$$

  5. The last $Es$ columns of the image $I_t$ is filled

$$\begin{aligned} &I_t'(1:1:M+2*Es, N+2*Es:-1:N+Es+1) \\ &= I_t'(1:1:M+2*Es, N+2*Es-Size+1:1:N+Es-1) \end{aligned} \quad (23)$$

- *Step 3*. The window is moved across each image $I_t$, the $Block_t^{(i,j)}$ centralizing at pixel $(i, j)$ is extracted and its covariance matrix $cov_t^{(i,j)}$ is solved.
- *Step 4*. The eigenvalues $V_t^{(i,j)}$ and the eigenvectors $D_t^{(i,j)}$ of each $Block_t^{(i,j)}$ are computed according to $Cov_t^{(i,j)}$.
- *Step 5*. The fusion coefficient $Weight_t^{(i,j)}$ at pixel $(i, j)$ in image $I_t$ is given by the following expression:

$$Weight_t^{(i,j)} = \frac{\sum_{p=1}^{2} \left| V_t^{(i,j)}(p,1) \right|}{\sum_{k=1}^{m} \sum_{p=1}^{2} \left| V_k^{(i,j)}(p,1) \right|} (t = 1,2,...,m) \quad (24)$$

- *Step 6*. $m$ images are merged at pixel $(i, j)$ in image $I$.

$$I(i,j) = \sum_{t=1}^{m} I_t(i,j) \bullet Weight_t^{(i,j)} \quad (25)$$

## 6. Experiments and Results

In this paper, the experiments are performed in MATLAB 7.1 on PC with an Intel Dual-Core E5500 2.80GHz and 2GB RAM, running Windows XP. In the following registered images, the red and green landmarks express the results from extracting the edges of the reference and floating images by canny operator

respectively, and the yellow landmarks label the overlapping region of two registered images. In order to assess the registration accuracy, we use error $\rho_i$ [16].

$$\rho_i = \frac{|\Delta i - \Delta i_S|}{|\Delta i_S|} \times 100\% \qquad (i = x, y, \theta) \qquad (26)$$

Where $\Delta i_s$ denotes the standard transformation parameter aligning the moving image with the static image, and $\Delta i$ implies the actual transformation parameter computed by the registration method. Besides, we introduce total error $\rho$ [16].

$$\rho = \sum_{i=\{x,y,\theta\}} \rho_i \qquad (27)$$

The experimental images are divided into the following four groups. The first is to select CT1 image as the static one and, MR1 as the moving image, whose sizes are of $256 \times 256$ pixels, shown in Figure 1.

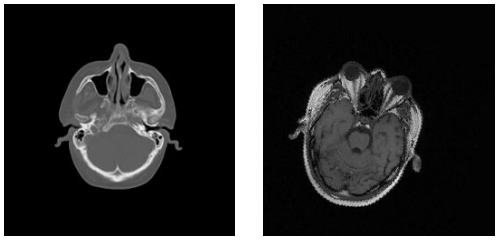

a) CT1 static image. b) MR1 moving image.

Figure 1. The first group.

The second is to select CT2 image as the static one and, PET1 as the moving image, whose sizes are of $128 \times 128$ pixels, shown in Figure 2.

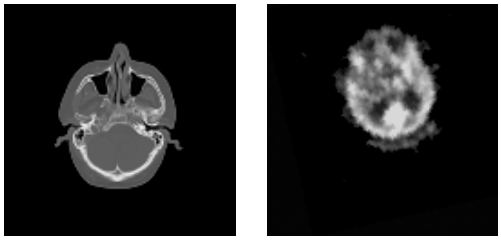

a) CT2 static image. b) PET1 moving image.

Figure 2. The second group.

The third is to select MR2 image as the static one and, PET2 as the moving image, whose sizes are of $128 \times 128$ pixels, shown in Figure 3.

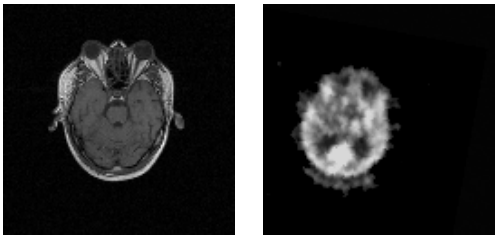

a) MR2 static image. b) PET2 moving image.

Figure 3. The third group.

And the last is to select MR3 image as the static one and, SPECT1 as the moving image, whose sizes are of $256 \times 256$ pixels, shown in Figure 4.

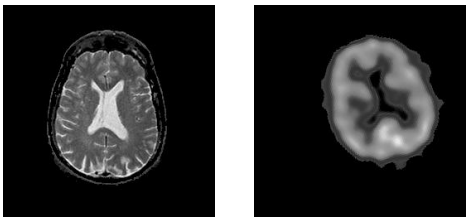

a) MR3 static image. b) SPECT1 moving image.

Figure 4. The fourth group.

Also, we list the relatively accurate transformation parameters in Table 1, which are taken as $\Delta i_s$ in Equation (11). The experimental images above are derived form the following two sources. One is from the brain image database founded by Retrospective Registration Evaluation Projection, which is affiliated to Vanderbilt University, USA. We extract CT Number 2, MR_T1 Number 2 and PET Number 5 brain images of the training_006 as the experimental images with gray level being 256. Another is from the web page: http://www.med.harvard.edu/AANLIB/cases/case 36/mr1-tc1/031.html.

Table 1. Transformation parameters of the moving images.

| Floating images | Parameters | | |
|---|---|---|---|
| | $\Delta x_s$ /Pixel | $\Delta y_s$ /Pixel | $\Delta \theta_s$ /° |
| **The first group** | -10 | 18 | -15.5 |
| **The second group** | 5 | -18 | 12.8 |
| **The third group** | -17 | 11 | -10.5 |
| **The fourth group** | 26 | -13 | 24.5 |

## 4.1. Multi-Modality Medical Image Registration

We first use ICP to implement the multi-modality medical image registration, and then use RPCA and RPCA-ICP to register the experimental images. The experimental results are illustrated in Figures 5, 6, 7, and Table 2.

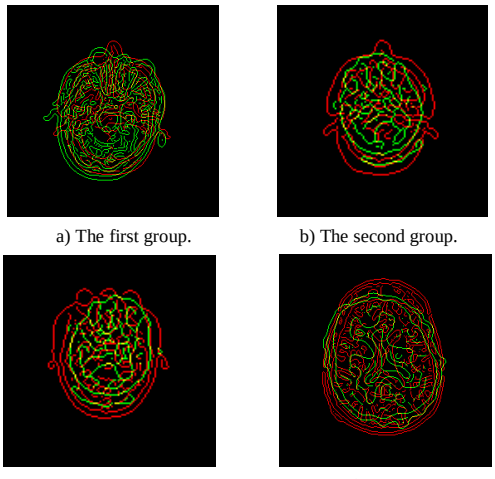

a) The first group. b) The second group.

c) The third group. d) The fourth group.

Figure 5. Registration result figures by ICP.

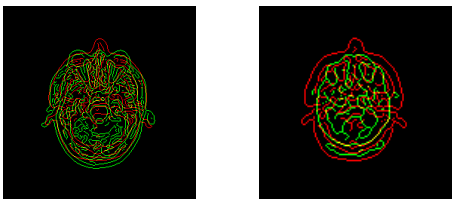

a) The first group. b) The second group.

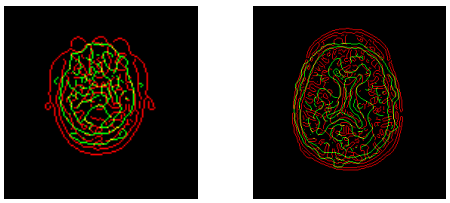

c) The third group. d) The fourth group.

Figure 6. Registration result figures by RPCA.

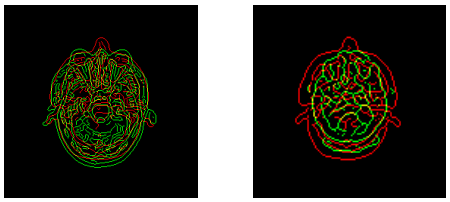

a) The first group. b) The second group.

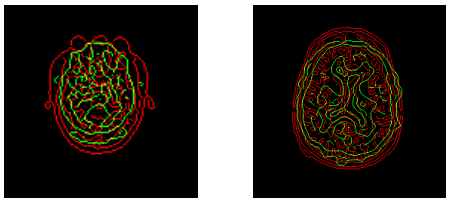

c) The third group. d) The fourth group.

Figure 7. Registration result figures by RPCA-ICP.

From Table 2, the registration speed of ICP is relatively more time-consuming, especially for registering the images of the first group; the processing time of RPCA is the shortest and almost negligible; for RPCA-ICP, although it is obviously superior to ICP, it is far inferior to RPCA. Further considering registration accuracy, ICP fully fails to register all the images and its translation transforma traps in the local optima; Although RPCA can successfully register all the images, we also can note that, the total errors produced by the alignments of the images of the second and fourth groups are relatively higher and need to further be improved; As for RPCA-ICP, it also can be successful in registering all the images and has a higher alignment accuracy, which is in accordance with the errors in Table 2. Therefore, the combination both avoids trapping into the local optima and advances the alignment accuracy. Also, RPCA has a higher accuracy in the rotation angle error but a lower one in the translation error; For RPCA-ICP, it has higher accuracies in both the rotation angle and the translation errors. Therefore, on the whole, RPCA-ICP can be effectively applied for the multi-modality medical image registration.

Table 2. Performance of registering the multi-modality images using ICP, RPCA and RPCA-ICP.

| Images | Registration methods | Parameters | | | | Errors | | | |
|---|---|---|---|---|---|---|---|---|---|
| | | $\Delta x_s$ /Pixel | $\Delta y_s$ /Pixel | $\Delta\theta_s$ /° | Time/S | $\rho_x$ | $\rho_y$ | $\rho_\theta$ | $\rho$ |
| **The first group** | **ICP** | -11.0514 | 16.6028 | -1.7789 | 28.0630 | 10.5140 | 7.7622 | 88.5232 | 106.7994 |
| | **RPCA** | -9.6463 | 18.395 | -15.864 | 0.266 | 3.5370 | 2.1944 | 2.3484 | 8.0798 |
| | **RPCA-ICP** | -9.8341 | 18.092 | -15.663 | 21.854 | 1.6590 | 0.5111 | 1.0516 | 3.2217 |
| **The second group** | **ICP** | 4.5945 | -16.5915 | 0.6051 | 0.9060 | 8.1100 | 7.8250 | 95.2727 | 111.2077 |
| | **RPCA** | 5.2940 | -18.5853 | 12.3681 | 0.219 | 5.8800 | 3.2517 | 3.3742 | 12.5059 |
| | **RPCA-ICP** | 4.8277 | -18.3688 | 12.5527 | 0.6880 | 3.4460 | 2.0489 | 1.9320 | 7.4269 |
| **The third group** | **ICP** | -19.8653 | 10.6694 | -1.6031 | 1.2810 | 16.8547 | 3.0055 | 84.7324 | 104.5926 |
| | **RPCA** | -16.831 | 11.7107 | -10.585 | 0.7540 | 0.9941 | 6.4609 | 0.8095 | 8.2645 |
| | **RPCA-ICP** | -16.580 | 11.4035 | -10.673 | 0.234 | 2.4706 | 3.6682 | 1.6476 | 7.7864 |
| **The fourth group** | **ICP** | 27.8957 | -11.3791 | 0.0114 | 3.766 | 7.2912 | 12.4685 | 99.9535 | 119.7132 |
| | **RPCA** | 27.6818 | -14.3565 | 24.2116 | 0.281 | 6.4685 | 10.4346 | 1.1771 | 18.0802 |
| | **RPCA-ICP** | 25.7056 | -12.5265 | 24.3429 | 3.0000 | 1.1323 | 3.6423 | 0.6412 | 5.4158 |

## 4.2. Multi-Modality Medical Image Fusion

In this section, in order to access and compare the methods, we use the entropy $H$ and the average cross entropy $J$ as the objective evaluation standards, which are defined by the following expresses [8, 20]

$$H(x) = -\sum_{i=0}^{255} p(i) log_2^{p(i)} \tag{28}$$

$$J(I) = \sqrt{\frac{1}{m}\sum_{t=1}^{m}\left(J_0(I, I_t)\right)^2} \tag{29}$$

here

$$J_0(I, I_t) = \sum_{i=0}^{255} p_I(i) log_2^{p_I(i)/p_{I_t}(i)} \tag{30}$$

$H$ reflects the mean information content in the fused image. $H$ is more, the fused image covers the much richer information. $J$ is a crucial performance index used for evaluating the difference between two images and directly reflects the corresponding pixel difference between two images. $J$ is less, the fusion effect is better. In the experiments, we use such the fusion methods as FPCA, FMPCA, Laplacian Pyramid, Gradient Pyramid, DWT (DBSS[2,2]) and SIDWT (Harr) to compare the fusion performances and the experimental results are as shown in Figures 8, 9, 10, 11, 12, 13, and Table 3.

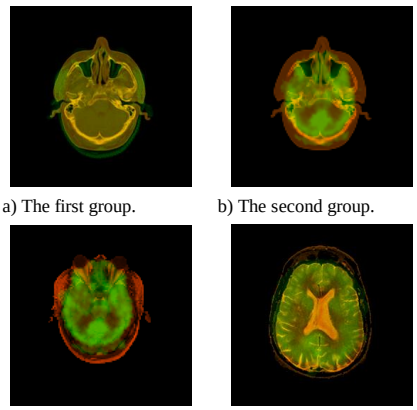

a) The first group. b) The second group.

c) The third group. d) The fourth group.

Figure 8. Fusion result figures by FPCA.

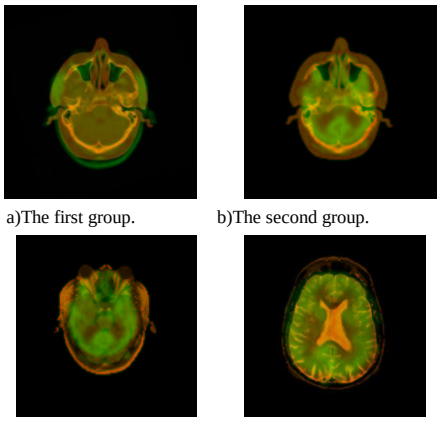

a)The first group. b)The second group.

c)The third group. d)The fourth group.

Figure 9. Fusion result figures by FMPCA.

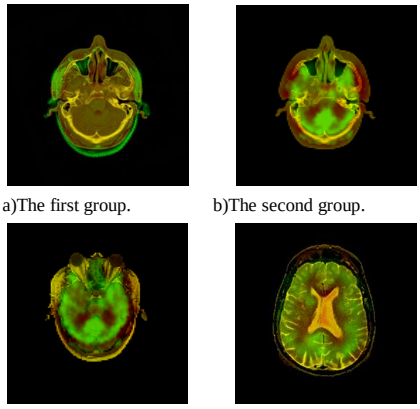

a)The first group. b)The second group.

c)The third group. d)The fourth group.

Figure 10. Fusion result figures by Laplacian Pyramid.

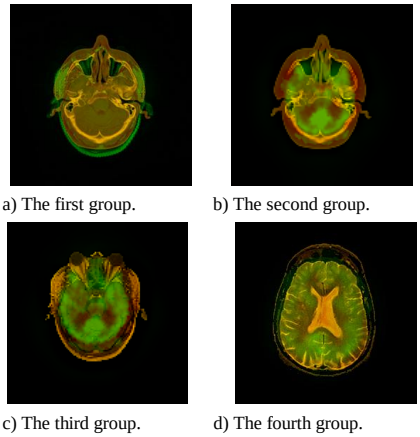

a) The first group. b) The second group.

c) The third group. d) The fourth group.

Figure 11. Fusion result figures by Gradient Pyramid.

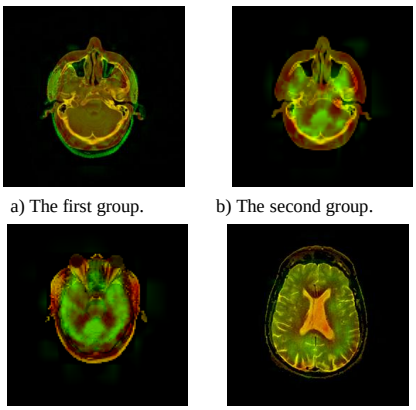

a) The first group. b) The second group.

c) The third group. d) The fourth group.

Figure 12. Fusion result figures by DWT (DBSS [2,2]).

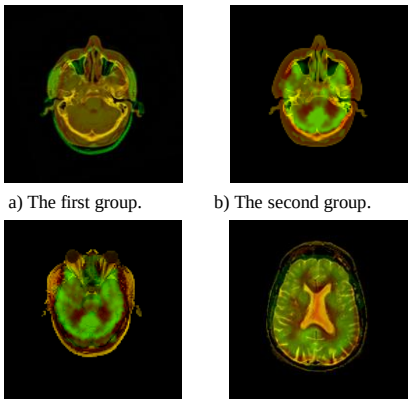

a) The first group. b) The second group.

c) The third group. d) The fourth group.

Figure 13. Fusion result figures by SIDWT (Harr).

Table 3. Comparisons of image fusion methods.

| Fusion Method | Index | Experimental Images | | | |
|---|---|---|---|---|---|
| | | First Group | Second Group | Third Group | Fourth Group |
| FPCA | *H* | 3.1261 | 2.4367 | 2.5558 | 3.0758 |
| | *J* | 0.9915 | 0.2941 | 0.1796 | 0.1682 |
| FMPCA | *H* | 3.7626 | 2.6546 | 2.6770 | 3.2959 |
| | *J* | 1.3996 | 0.2637 | 0.2139 | 0.1978 |
| Laplacian Pyramid | *H* | 3.6793 | 2.5654 | 2.5491 | 3.1824 |
| | *J* | 1.0429 | 0.1681 | 0.1136 | 0.0626 |
| Gradient Pyramid | *H* | 4.3349 | 3.9693 | 3.6939 | 3.8330 |
| | *J* | 1.3724 | 2.0204 | 1.6810 | 0.3330 |
| DWT(DBSS[2,2]) | *H* | 4.0442 | 3.4941 | 3.4927 | 3.4157 |
| | *J* | 1.0845 | 0.6528 | 0.7357 | 0.1254 |
| SIDWT(Harr) | *H* | 3.7065 | 2.5239 | 2.4838 | 3.1520 |
| | *J* | 1.1191 | 0.1896 | 0.1228 | 0.0853 |

From Figures 8, 9, 10, 11, 12, 13, and Table 3, considering the entropy *H*, FMPCA is superior to FPCA, Laplacian Pyramid and SIDWT (Harr), but is inferior to Gradient Pyramid and DWT (DBSS[2,2]). From the point of view of the average entropy *J*, FMPCA surpasses Gradient Pyramid except for fusing the images in the first group and DWT (DBSS[2,2]) except for fusing the images in the second and third groups, but it is worse than FPCA except for fusing the images in the second group and DWT (DBSS[2,2]) except for fusing the images in the first and fourth groups; In addition, for all the four groups, FMPCA is inferior to Laplacian Pyramid and SIDWT (Harr). Therefore, in general, the fusion performance of FMPCA is superior to that of FPCA, is similar to

those of Laplacian Pyramid and SIDWT (Harr), but inferior to those of Gradient Pyramid and DWT (DBSS[2,2]).

## 7. Conclusions

In this paper, we discuss the application of PCA to medical image registration and fusion. When aligning the images, the image moments are used to obtain the centroids of the registering images and the same time the translation values are derived, and then the rotation angle values are computed by PCA, finally the image registration is implemented. Due to the existing problems of ICP, we combine PCA with ICP to register the images, namely, the translation and rotation values acquired by PCA are viewed as the initial parameters for ICP, which is conducive to further boosting the registration accuracy. The experimental results show that the combination has a simple implementation, a low computational load, higher registration accuracy, and a remarkable ability that avoids easily getting into the local optimum. When merging the images, according to the sub-block extracted by the moving window in each fusing image, the covariance matrix first and then the eigenvectors are solved by PCA, and then the fusion coefficient of the sub-block at its central pixel is computed, finally the fused image is created. The experimental consequences reveal that FMPCA is superior to FPCA.

## Acknowledgement

This work is supported by Hunan Provincial Natural Science Foundation of China (No. 2016JJ2093), supported by Hunan University of Arts and Science, Hunan Province Cooperative Innovation Center for The Construction & Development of Dongting Lake Ecological Economic Zone, and supported by the Construct Program of the key Discipline in Hunan University of Arts and Science. The authors declare that there is no conflict of interest regarding the publication of this manuscript.

## References

[1] Arun K., Huang T., and Blostein S., "Least-Squares Fitting of Two 3-D Point Sets," *IEEE Transactions on Pattern Analysis and Machine Intelligence*, vol. 9, no. 5, pp. 698-700, 1987.

[2] Besl P. and Mckay N., "A Method for Registration of 3-D Shapes," *IEEE Transactions on Pattern Analysis and Machine Intelligence*, vol. 14, no. 2, pp. 239-256, 1992.

[3] Can A., Stewart C., Roysam M., and Tanenbaum H., "A Feature-Based, Robust, Hierarchical Algorithm for Registration Palm of Images of the Curved Human Retina," *IEEE Transactions on Pattern Analysis and Machine Intelligence*, vol. 24, no. 3, pp. 347-364, 2002.

[4] Daneshvar S. and Ghassemian H., "MRI and PET Image Fusion by Combining IHS and Retina-Inspired Models," *Information Fusion*, vol. 11, no. 2, pp. 114-123, 2010.

[5] Gulrez T. and Al-Odienat A., "A New Perspective On Principal Component Analysis Using Inverse Covariance," *The International Arab Journal of Information Technology*, vol. 12, no. 1, pp. 104-109, 2015.

[6] Hu M., "Visual Pattern Recognition by Moment Invariants," *IRE Transactions on Information Theory*, vol. 8, no. 2, pp. 179-187, 1962.

[7] Kaneko S., Kondo T., and Miyamoto A., "Robust Matching of 3D Contours Using Iterative Closest Point Algorithm Improved by M-Estimation," *Pattern Recognition*, vol. 36, no. 9, pp. 2041-2047, 2003.

[8] Laliberte F., Gagnon L., and Sheng Y., "Registration and Fusion of Retinal Images-An Evaluation Study," *IEEE Transactions on Medical Imaging*, vol. 22, no. 5, pp. 661-673, 2003.

[9] Li S., Yang B., and Hu J., "Performance Comparison of Different Multi-Resolution Transforms for Image Fusion," *Information Fusion*, vol. 12, no. 2, pp. 74-84, 2011.

[10] Liu W. and Ribeiro E., "Incremental Variations of Image Moments for Nonlinear Image Registration," *Signal, Image and Video Processing*, vol. 8, no. 3, pp. 423-432, 2014.

[11] Liu Y., Cheng H., Huang J., Zhang Y., Tang X., and Tian J., "An Effective Non-rigid Registration Approach for Ultrasound Image Based on 'Demons' Algorithm," *Journal of Digital Imaging*, vol. 26, no. 3, pp. 521-529, 2013.

[12] Maintz J. and Viergever M., "A Survey of Medical Image Registration," *Medical Image Analysis*, vol. 2, no. 1, pp. 1-36, 1998.

[13] Miao Q., Shi C., Xu P., Yang M., and Shi Y., "A Novel Algorithm of Image Fusion Using Shearlets," *Optics Communications*, vol. 284, no. 6, pp. 1540-1547, 2011.

[14] Naidu V. and Raol J., "Pixel-Level Image Fusion Using Wavelets and Principal Component Nalysis," *Defence Science Journal*, vol. 58, no. 3, pp. 338-352, 2008.

[15] Nejati M. and Pourghassem H., "Multiresolution Image Registration in Digital X-Ray Angiography with Intensity Variation Modeling," *Journal of Medical Systems*, vol. 38, no. 1, pp. 10-18, 2014.

[16] Pan M., Jiang J., Rong Q., Zhang F., Zhou H., and Nie F., "A Modified Medical Image Registration," *Multimedia Tools and Applications*, vol. 70, no. 3, pp. 1585-1615, 2014.

[17] Park H., Bland P., Brock K., and Meyer C., "Adaptive Registration Using Local Information Measures," *Medical Image Analysis*, vol. 8, no. 4, pp. 465-473, 2004.
[18] Wang Z., Ma Y., and Gub J., "Multi-Focus Image Fusion using PCNN," *Pattern Recognition*, vol. 43, no. 6, pp. 2003-2016, 2010.
[19] Wong R., "Scene Matching with Invariant Moments," *Computer Graphics and Image Processing*, vol. 8, no. 1, pp. 16-24, 1978.
[20] Yang L., Guo B., and Ni W., "Multimodality Medical Image Fusion Based on Multiscale Geometric Analysis of Contourlet Transform," *Neurocomputing*, vol. 72, no. 3, pp. 203-211, 2008.

**Meisen Pan** was born in 1972 and graduated from Hunan Normal University, China, in 1995. He received the M.S. degree from Huazhong University of Science and Technology, China, in 2005. He obtained the Ph.D. degree from Central South University, China, in 2011. He has published more than 30 papers on journals and conferences. His research interests include biomedical image processing, information fusion and software engineering.

**Jianjun Jiang** was born in 1971 and graduated from Hunan University of Arts and Science, China, in 2010. She has published 2 papers on journals and conferences. Her research interests include image processing and information retrieves.

**Fen Zhang** was born in 1972 and graduated from Hunan University, China, in 1996. He received the M.S. degree from Hunan University, China, in 2005. He has published more than 10 papers on journals and conferences. His research interests include image processing and computer graphics.

**Qiusheng Rong** was born in 1973 and graduated from Central China Normal University, China, in 1996. He received the M.S. degree from Central China Normal University of Science and Technology, China, in 2001. He has published more than 10 papers on journals and conferences. His research interests include data mining and image processing.